Electron Transport and Recombination in ZnO-Based Dye-Sensitized Solar Cells

ARTICLE *in* THE JOURNAL OF PHYSICAL CHEMISTRY C · NOVEMBER 2011

Impact Factor: 4.77 · DOI: 10.1021/jp206698t

3 AUTHORS, INCLUDING:

E. Guillén
Abengoa
29 PUBLICATIONS **709** CITATIONS
SEE PROFILE

Juan A Anta
Universidad Pablo de Olavide
109 PUBLICATIONS **1,799** CITATIONS
SEE PROFILE

THE JOURNAL OF PHYSICAL CHEMISTRY C

ARTICLE

pubs.acs.org/JPCC

Electron Transport and Recombination in ZnO-Based Dye-Sensitized Solar Cells

E. Guillén,[†] L. M. Peter,[‡] and J. A. Anta*[,†]

[†]Departamento de Sistemas Físicos, Químicos y Naturales, Universidad Pablo de Olavide, 41013 Sevilla, Spain

[‡]Department of Chemistry, University of Bath, Bath BA2 7AY, United Kingdom

Supporting Information

ABSTRACT: The photovoltaic performance of ZnO-based dye-sensitized solar cells (DSCs) has been studied for three different configurations involving two dyes and two types of electrolytes with the iodide/iodine as redox mediator: ZnO/N719/organic solvent electrolyte (C1), ZnO/D149/organic solvent electrolyte (C2), and ZnO/N719/ionic liquid electrolyte (C3). The DSCs were characterized by measuring current−voltage curves and photovoltage as a function of light intensity and by electrochemical impedance spectroscopy (EIS), intensity-modulated photocurrent spectroscopy (IMPS), intensity-modulated photovoltage spectroscopy (IMVS), and open circuit photovoltage decay (OCVD). The results demonstrate the good light harvesting properties of the D149 dye and highlight the photovoltage limitation of the solvent-free (ionic liquid) electrolyte. The intensity dependence of the photovoltage and the OCVD, EIS, and IMVS results provide evidence of the nonlinear character of the recombination kinetics. It has been found that by combining EIS and IMPS data it is possible to overcome the problem of transport resistance determination for cells where there is no clear transmission line feature in the impedance measurements. The resulting electron diffusion lengths (L_n) indicate good electron collection for all studied cells, pointing to poor injection as the main limitation in DSCs based on the ZnO semiconductor.

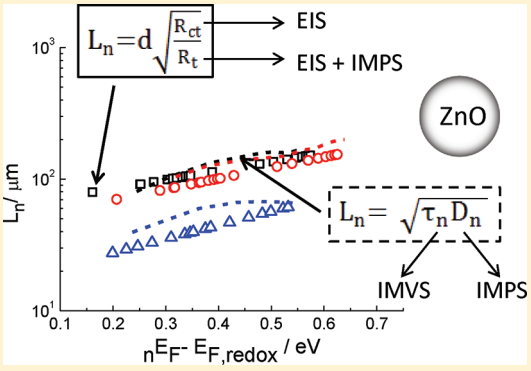

1. INTRODUCTION

ZnO was one of the first materials employed in dye solar cells.[1,2] It was also the first nanoporous semiconductor used as a working electrode for this type of device.[3] The band gap and conduction band edge of ZnO are similar to that of TiO_2.[4,5] The electron mobility, at least in single crystals, is more than 1 order of magnitude larger in ZnO than in TiO_2 (anatase).[6−8] However, despite many efforts to improve the efficiency of ZnO based dye solar cells, it remains lower than that for TiO_2 based cells. The best efficiency for a ZnO dye-sensitized solar cell up to now was achieved by Saito and Fujihara,[9] who obtained 6.58% for AM 1.5 conditions. This is around half of the best efficiency obtained for TiO_2.[10] ZnO allows for easy fabrication of a very wide range of nanostructures by means of different synthetic routes.[11,12] However, it exhibits poor chemical stability compared with TiO_2. The low performance of ZnO cells sensitized with the most common ruthenium-based dyes has been ascribed to partial dissolution of the ZnO surface and formation of dye aggregates.[13]

The majority of studies regarding ZnO solar cells have been focused on two main aspects: (1) exploiting the ease of preparing one-dimensional nanostructures with attractive conducting properties,[14−16] and (2) searching for suitable dyes for this semiconductor.[17−19] However, in comparison with TiO_2, fewer detailed studies of electron transport and recombination have been carried out on dye-sensitized nanostructured ZnO solar cells.[20−22]

The principal objective of this study was to gain deeper insight into the behavior of ZnO-based solar cells, paying special attention to its electronic properties, and examining whether the theoretical approaches developed for mesoporous TiO_2 (multiple-trapping transport in an exponential distribution of localized states,[23,24] nonlinear recombination,[25,26] etc.) can be applied to ZnO-based DSCs. Furthermore, we aimed to identify the factors responsible for the lower performance of ZnO-based solar cells, so that strategies for improvement can be formulated. We therefore tested different dyes and electrolytes in order to find properties that are intrinsically dependent on the semiconductor oxide and not on the other components of the cell. In this regard, it must be pointed out that recent publications[27−29] have highlighted the importance of loss processes such as inefficient injection or dye regeneration in DSCs. These processes could affect the performance of ZnO devices, as it will be discussed here.

In this study we have used a comprehensive set of characterization techniques, including standard measurements of current−voltage curves and incident photon-to-current efficiency (IPCE) measurements, but also small-perturbation techniques and open circuit voltage decay (OCVD) for probing transport and recombination. As regards small-perturbation techniques, it has been

Received: July 14, 2011
Revised: September 27, 2011

   dx.doi.org/10.1021/jp206698t | J. Phys. Chem. C XXXX, XXX, 000–000

previously reported[30,31] that impedance spectroscopy alone is not adequate to extract transport properties and electron diffusion lengths in ZnO-based DSCs as the transmission line feature is not clearly visible in the spectrum. In this work we have devised an alternative method to obtain the electron diffusion length in these cells by combining impedance spectroscopy and intensity modulated photocurrent spectroscopy (IMPS). To combine the different techniques, appropriate corrections were applied to ensure the relevant parameters (lifetimes, diffusion lengths, etc.) are obtained for the same electronic conditions (same position of the Fermi level with respect to the conduction band). The good agreement found between the different techniques for the electron lifetimes and diffusion lengths provide definitive evidence that ZnO-based DSC exhibits nonlinear recombination features analogous to those found in typical TiO_2 solar cells and that electron collection is very efficient, approaching 100% even for cells with ionic liquid electrolyte. This result suggests that other factors such as low injection efficiency must be responsible of the limited efficiency of ZnO-based DSCs.

2. EXPERIMENTAL METHODS

Fabrication of Dye-Sensitized Solar Cells. The dye-sensitized ZnO photoanodes used in this work were fabricated on fluorine-doped tin-oxide-coated glass substrates (TEC15, Pilkington). Thin continuous ZnO blocking layers were deposited from a zinc acetate solution (0.1 M Zn $[C_2H_3O_2]\cdot 2H_2O$, 0.2 M $C_2H_4O_6$ in 25:75 (v/v) water/ethanol mixture) by spray pyrolysis. During deposition the substrate was held at ∼350 °C. The precursor was sprayed in 15 consecutive 2 s bursts with a pause between each burst of 8 s.[32] The ZnO paste for the semiconductor electrodes was prepared by mixing Evonik VP AdNano@ZnO20 (approximate nanoparticle size of 20 nm) and PI-KEM (approximate nanoparticle size of 50 nm) in 1:1 proportion. The nanopowder mixture was dispersed in water and ethanol (30:70) and stirred overnight to obtain a colloidal suspension of 30 wt %. For thin film preparation the suspension was spread onto the substrate with a glass rod using Scotch tape as spacer. The resulting film was then heated at 420 °C for 30 min. The film thickness after sintering was around 8 μm, and the active area of the cells was 0.64 cm^2.

Two different dyes were used for semiconductor sensitization. For configurations 1 (C1) and 3 (C3), the films were immersed in an ethanolic solution 0.5 mM of the Ru-based dye known as N719 (Solaronix) for 1 h. For configuration 2 (C2), the sensitization was performed by immersing the electrodes in a solution of 0.5 mM D149 (Mitsubishi Paper Mills Limited) and of 0.7 mM chenodeoxycholic acid in *tert*-butyl alcohol−acetonitrile (1:1) for 30 min. The photoanodes were then rinsed with the same solvents used for sensitization. Platinized counter electrodes were fabricated on TEC8 electrodes (Pilkington) by spreading 15 μL of Platisol (Solaronix) and subsequent annealing at 400 °C for 5 min. Two small filling holes were previously drilled in the FTO glass. Photoanodes and counter electrodes were sealed together in a sandwich configuration using a hot-melt polymer (Solaronix, SX1170-25). The space between the electrodes was vacuum filled with the electrolyte. The electrolyte solutions employed were as follows: C1, 0.5 M LiI, 0.05 M I_2, and 0.5 M TBP in 3-methoxypropionitrile; C2, 0.5 M TBAI, 0.05 M I_2, in acetonitrile/ethylenecarbonate, 1:4; C3 (solvent free), 0.05 M I_2 in 1-ethyl-3-methyl-imidazolium tetracyanoborate (EMIBCN) and 1-propyl-3-methyl-imidazolium iodide (PMIMI) (35:65 vv). At least three cells of each type were fabricated. The combination of the D149 dye and the ionic liquid electrolyte was not used as D149 dye desorbs in the presence of the ionic liquid.[30]

Table 1. $I-V$ Characteristics of the Solar Cells Studied in This Work

sample	J_{sc} (mA/cm^2)	V_{oc} (V)	FF	η (%)
C1(ZnO/N719/OLE)	7.21	0.63	0.53	2.47
C2(ZnO/D149/OLE)	10.04	0.61	0.43	2.67
C3(ZnO/N719/ILE)	7.07	0.52	0.52	1.95

Characterization Techniques. The illumination source for current−voltage characteristics was a xenon arc lamp with an AM 1.5 spectral filter. A calibrated silicon solar cell with an IR filter (KG5) was used to adjust the light intensity to 1 sun (100 mW/cm^2). The KG5 filter provides a closer match of the reference cell to the DSC spectral response.[33] Incident photon-to-current-efficiency (IPCE) measurements were made using a 150 W xenon lamp in combination with a grating monochromator and calibrated with a silicon photodiode. Impedance spectroscopy (EIS) measurements under illumination and intensity-modulated spectroscopies (IMPS and IMVS) were carried out using a Solartron 1250 frequency response analyzer (FRA) and a Solartron 1286 electrochemical interface. The illumination for the frequency response techniques was provided by a 530 nm LED over a wide range of dc light intensities. EIS measurements were performed using a 10 mV perturbation in the $10^{-2}-10^{5}$ Hz range. The amplitude of the sinusoidal modulation for IMVS and IMPS measurements was 10% of the dc illumination. Zview equivalent circuit modeling software (Scribner) was used for fitting impedance spectra. To obtain the short circuit voltage (V_{sc})[34] data, the solar cell was illuminated under short circuit conditions with the 530 nm LED. In this technique, the LED is switched off and the cell is switched to open circuit simultaneously, while the voltage is monitored by an oscilloscope. Open circuit voltage decay (OCVD) measurements were made using a high impedance low noise preamplifier and an oscilloscope. The dependence of the photovoltage on intensity was determined by illuminating the cells with the green diode laser (532 nm). The intensity of the light was varied using Schott NG neutral density filters.

3. RESULTS AND DISCUSSION

3.1. Photovoltaic Performance. Table 1 shows the $I-V$ characteristics (AM 1.5) for one representative cell of each configuration. C2 exhibits the highest short circuit current (J_{sc}), which can be attributed, in part at least, to the larger absorption coefficient of D149 compared to N719.[35] In C2 and C3 the same dye (N719) is employed but for C3 a higher viscosity electrolyte is used. Diffusion limitations are often observed in pure ionic liquid electrolyte cells,[36] and therefore, J_{sc} was expected to be lower for C3 than for C1. However, both types of cells exhibited a similar J_{sc}, indicating that slow diffusion in the electrolyte is not a significant limiting factor in C3 (probably because the current lies below the limiting diffusion current in this case[36]). Open circuit voltages (V_{oc}) are higher for C1. This result was expected due the presence of *tert*-butylpyridine (TBP) in the electrolyte. This additive has proved to have a positive effect in the photovoltage of DSCs,[23] including ZnO-

dx.doi.org/10.1021/jp206698t |*J. Phys. Chem. C* XXXX, XXX, 000–000

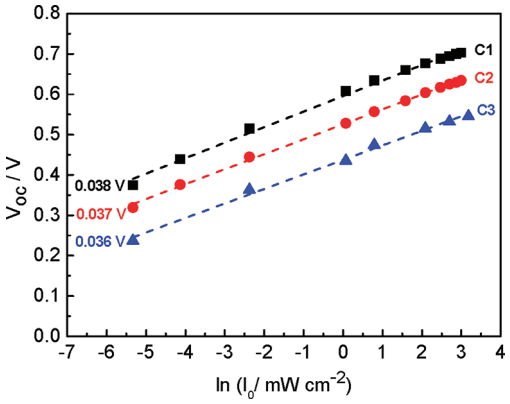

Figure 1. Semilogarithmic plots of open circuit voltage vs light intensity for solar cells studied in this work. Slopes in V are indicated in the graph.

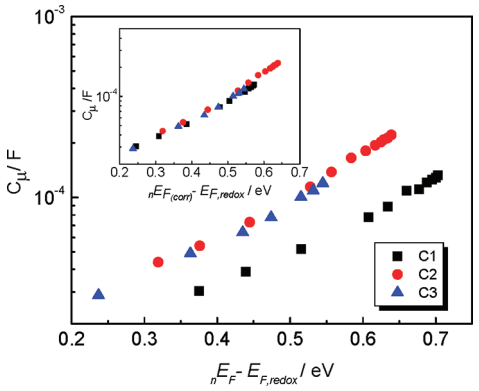

Figure 2. Capacitance values obtained from EIS fitting. The inset shows the results after band edge correction for configuration C1 (see text for details).

based solar cells.[37] On the other hand, as expected, C3 gives the lowest V_{oc}. Low voltages are usually reported in the literature for pure ionic liquid based electrolytes.[36] The fill factors for all three types of cell are about 0.5, similar to those previously reported for ZnO-based DSCs,[31] especially when high photocurrents are obtained. Even the most efficient ZnO-based solar cell obtained up to now (reported by Saito and Fujihara in 2008[9]) exhibits a fill factor of only 0.58. Also Quintana et al.,[38] when comparing TiO_2 and ZnO based cells with similar characteristics (same particle size, same electrolyte and same dye) found that ZnO cells have considerably lower fill factors (0.49) with respect to TiO_2 cells (0.69).

The best performing cell, as a consequence of its much higher J_{sc}, is C2. The peak incident photon-to-current efficiencies, IPCEs (see Figure S1 in the Supporting Information), are around 70% for C1 and 30% for C1 and C2 at the maximum of the dye absorption. The IPCE depends on the product of the efficiencies for light harvesting, injection, and electron collection. Good light harvesting properties have been reported for ZnO films sensitized with D149.[31] On the basis of the absorbance of the sensitized films and the AM1.5 solar spectrum, short circuit currents of 13.6 mA/cm^2 are predicted for C2, assuming 100% injection and collection efficiency. Therefore, the lower J_{sc} and IPCE for C2 point to poor collection efficiency and/or inefficient injection from the dye. N719 has a narrower absorption spectrum and small absorption coefficient than D149, so a lower light harvesting is expected. Dye loading measurements give 8×10^{-8} mol/cm^2 for this dye, which would produce a maximum current of ~10.6 mA/cm^2 for 100% injection and collection efficiency. Furthermore, it is well-known that N719 can produce degradation of the ZnO films by formation of Zn^{2+} aggregates.[37] Despite the D149 dye having an acidic group, it has been observed previously[30] that this dye does not produce deterioration of the ZnO photoanodes utilized in this study.

3.2. Light Intensity Dependence of the Open Circuit Voltage. The semilogarithmic plots in Figure 1 show the light intensity dependence of the open circuit voltage V_{oc}. For the three samples V_{oc} depends linearly on the logarithm of the light intensity according to

$$V_{oc} \propto \frac{mk_BT}{q} \ln(I_0) \qquad (1)$$

where k_B is the Boltzmann constant, T the temperature, and q the elementary charge. The parameter m is an empirical nonideality factor. All three types of cells depart from ideal-diode behavior, with nonideality factors higher than 1 (see Table 2 and Figure 1). DSCs usually behave nonideally (see ref 25 and references therein), although the origin of this nonideality is not clearly understood. It is often attributed to recombination via surface states.[39] In this case the density of electrons available for transfer to the redox couple varies with Fermi level in a way that depends on the surface state energy distribution. A reaction order (β) lower than 1 is an empirical way of describing sublinear recombination kinetics that take into account that electrons may be transferred from occupied levels located in the energy gap.[25,26] If this is the only source of nonideality, the ideality factor m is related to the reaction order through its inverse, $m = 1/\beta$, so that $\beta \sim 0.7$ for the three configurations. The reaction order can also be estimated from the slope of the charge-transfer resistance versus voltage in an EIS experiment.[25] This approach is discussed below. Nonideality has also been attributed to a nonideal dependence of the Fermi level on the density of conduction band electrons (introduced via an electron activity coefficient)[40] or to a shift in the conduction band when the electron concentration is varied.[41] The steady-state electron concentration may be also affected by back reaction via the substrate. However, the linearity of the response of the V_{oc} versus logarithmic of the light intensity plot is an indication that recombination through the substrate is negligible over the entire range of measured photon fluxes and that the sprayed blocking layer is working properly.[42]

3.3. Electrochemical Impedance Spectroscopy Studies. EIS measurements of the devices were made at open circuit under illumination over a wide range of light intensities. As indicated above, all samples were studied under the same illumination conditions. All the impedance spectra show the characteristic midfrequency semicircle that arises from charge transfer in the oxide−electrolyte interface (see Figure S2 in the Supporting Information). In the case of C3, the spectrum shows a clear third semicircle (at low frequencies and high light intensities) that accounts for ionic diffusion in the electrolyte. Impedance spectra for C1 and C2 were fitted to the equivalent circuit also shown in Figure S2 in the Supporting Information. For C3, the charge transfer resistance and the interface capacitance were obtained directly by fitting the second semicircle to a single RC circuit.

The capacitance measured in TiO_2 by EIS usually shows an exponential variation with applied potential, corresponding to a trap energy distribution below the conduction band

dx.doi.org/10.1021/jp206698t |J. Phys. Chem. C XXXX, XXX, 000–000

Table 2. Characteristic Parameters of Transport and Recombination of the Solar Cells Studied in This Work

cell	V_{oc} vs light (V)	m	$1/m$	α	T_0 (K)	β (from R_{ct} fitting)	inverse slope $R_t$vs E_f (V)
C1	0.038	1.46	0.68	0.11	2700	0.64	0.035
C2	0.037	1.42	0.70	0.13	2300	0.59	0.037
C3	0.036	1.38	0.72	0.12	2500	0.69	0.033
ideal	0.026	1	1				0.026

edge.[43] This distribution is governed by the parameter α ($\alpha = T/T_0$, where T_0 is the characteristic temperature of the distribution)

$$C_\mu = C_0 \exp\left(\alpha \frac{({}_nE_F - E_{F,redox})}{k_B T}\right) \quad (2)$$

The capacitance values obtained for the three configurations of ZnO solar cells also show this exponential behavior (see Figure 2). However, as reported previously[31,36] the capacitance for ZnO solar cells exhibits a weak dependence on the Fermi level, with α ranging between 0.11 and 0.13 for the three configurations, whereas typical values of α in TiO_2 solar cells range between 0.2 and 0.4.[23,24] In contrast to previous results reported in the literature[44] we do not observe a clear dependence of this parameter on the electrolyte composition.

These results suggest an exponential trap energy distribution of ZnO with a very high characteristic temperature (much higher than in the case of TiO_2). Quintana et al.[38] also found a similar behavior for ZnO-based solar cells. From their charge extraction measurements, a trap distribution parameter $\alpha = 0.13$ is obtained. We have also considered whether this weak dependence of the capacitance could be related to an upward shift of the band edge due to electron accumulation. This possibility has been discussed recently for TiO_2 cells.[27] In that work it is predicted that band unpinning would lead to a curvature of the capacitance in the semilogarithmic plot. However, our capacitance results fit reasonably well to eq 2 with no evidence of curvature. The integrated electron charge obtained from capacitance data for C2 and an estimation of the band edge shift that would be produced by the accumulated electrons can be found in the Supporting Information (Figure S3).

Band bending due to space charge effects as discussed by Quintana et al.[38] seems also unlikely. These authors assumed that the donor density is equal to the charge obtained from their charge extraction measurements. Even if this assumption is made, the accumulated charged measured in our samples (Figure S3, Supporting Information) is almost 1 order of magnitude smaller, indicating that there is no significant band bending.[38,45]

The comparison of transport and recombination rates between different DSCs can only be made if the ratio of the number of electrons in the conduction band and in the traps is the same for all the samples.[46] For cells with similar trap distributions (as it is expected for C1, C2, and C3 considering they have a similar α), this condition is fulfilled when the position of the quasi Fermi level relative to the conduction band edge (${}_nE_F - E_c$) is set to equivalent values in the cells being compared. Under open circuit conditions we can assume that the electron quasi Fermi level through the film is essentially uniform. The energy of the conduction band edge can be shifted as a consequence of the interaction of the oxide with the surrounding electrolyte. This kind of displacement, which has been reported a number of times in the literature,[47] is illustrated in Scheme 1. When samples are compared with a similar trap distribution, the chemical capacitance data help to

Scheme 1. Illustration of the Band Edge Shift Produced by the Electrolyte in Configuration C1 (shown for the same value of conduction band electron density)

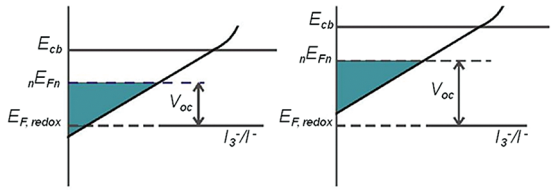

detect shifts in the conduction band edge.[48,49] In the present work the displacements observed in the capacitance data were taken into account to allow proper comparison of the different cells. Alternatively, if the diffusion coefficient of free electrons is considered to be constant, the transport resistance can be also used to estimate this displacement.[50] In fact, similar displacement values were obtained from the transport resistance data (see below).

In Figure 2, we observe an upward displacement of the ZnO conduction band for C1. This behavior can be attributed to the presence of TBP in the electrolyte.[48] The data for C1 have therefore been shifted by 130 mV (see inset Figure 2) in order to obtain the overlap of the capacitance values for the three kind of cells.[49] Taking this shift into account for configuration C1 allows us to compare the electron properties of the three configurations based on different dyes and electrolytes[50] at the same values of ${}_nE_F - E_c$.

It is important to note that the transmission-line feature commonly attributed to electron transport in the semiconductor oxide[24,48,51] is not observed in the spectra of the ZnO cells (Figure S2, Supporting Information). For this reason, reliable fitting of this parameter was difficult or in some cases impossible. The absence of the transport feature may reflect the higher mobility of electrons in ZnO in comparison to TiO_2.[52] At high voltages the transport resistance versus voltage plot obtained from the fittings is flattened off (see Figure S7, Supporting Information). Wang and Peter[44] also found this flattening when fitting the transport resistance from impedance measurements for TiO_2 cells under illumination and under high light intensity conditions. These authors concluded that when the value of R_t goes below the resistance of the cathode, fitting becomes unreliable. For ZnO cells, the transport resistance is not distinguishable from the cathode feature at any bias potential. A strategy to overcome this problem involving IMPS measurements in the fitting will be described below.

Charge transfer resistance R_{ct} data have been corrected by taking into account the band shift for C1 observed in the capacitance plots. The charge transfer resistances for C1, C2, and C3 versus ${}_nE_{F(corr)}$ are plotted in Figure 3. C3 has the lowest charge transfer resistance, which explains the difference of more than 100 mV of the photovoltage for this cell with respect to cell C2 (it must be born in mind that both cells have the conduction band at approximately the same energy according to Figure 2).

dx.doi.org/10.1021/jp206698t |J. Phys. Chem. C XXXX, XXX, 000–000

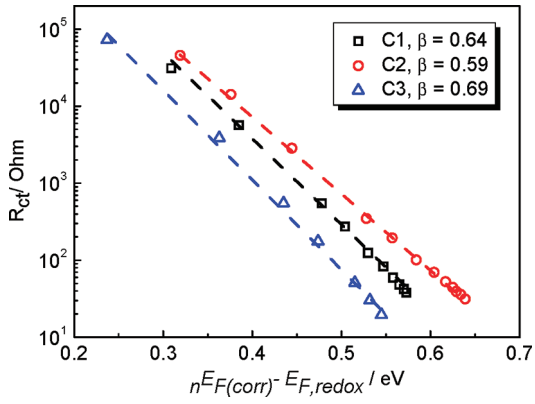

Figure 3. Charge transfer resistance obtained by fitting EIS spectra at various open circuit voltages. Note that data for C1 has been corrected for band displacement according to the capacitance data of Figure 2.

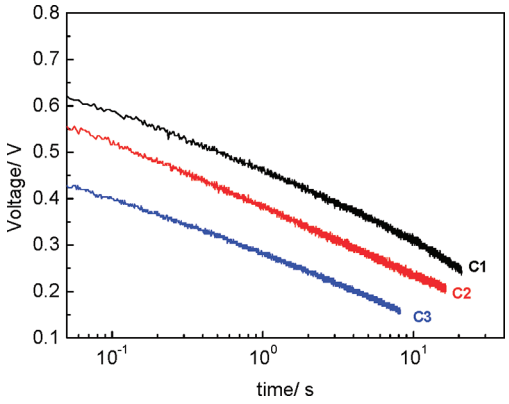

Figure 4. Open circuit voltage decays for the three configurations studied.

On the other hand, C1 exhibits slightly faster recombination than C2. The difference in open circuit voltage between C1 and C2 can be explained as a consequence of the difference in the position of the conduction band observed in the capacitance measurements as well as to the difference in the recombination resistance.

The charge transfer resistance contains primary information regarding the recombination rate under steady-state conditions.[53] The charge-transfer resistances show an exponential behavior in practically all the studied range

$$R_{ct} = R_0 \exp\left(-\beta \frac{({}_nE_F - E_{F,redox})}{k_B T}\right) \quad (3)$$

In eq 3, β can be considered[25] an empirical estimation of the reaction order in sublinear recombination kinetics. The fit of the R_{ct} versus voltage plots yields a β of 0.64, 0.59, and 0.69 for C1, C2, and C3 respectively. As already mentioned, the reaction order (in the absence of other sources of nonideality) is related to the nonideality factor m obtained from the V_{oc} vs $\ln(I_0)$ plot, $\beta = 1/m$.[25] As shown in Table 2, this relation is almost satisfied for C1 and C3, but not for C2. This could be an indication that other factors (discussed below) contribute to the nonideal behavior apart from a nonlinear recombination. For example, the parameter m could also include effects due to the nonideal behavior of electrons in the conduction band (departure from Boltzmann statistics of the free electron density).[40,41,54]

The lower V_{oc} obtained for C3 could also be a consequence of a displacement of the equilibrium redox potential of the I^-/I_3^- couple.[36] Taking into account that the molar iodide concentration in configuration C3 is much larger (2.4 M) than in the other two (0.5 M), the redox potential of the electrolyte is shifted toward more negative values. For fixed Fermi level in the semiconductor, this displacement leads to a lower photovoltage. However, using Nernst equation for a two-electron redox process, only a 20 mV displacement of the redox equilibrium level is predicted between the organic liquid electrolytes (C1, C2) and the ionic liquid electrolyte (C3).

In Figure 3 we can observe that the slope for C2 is slightly different from the other two configurations. This suggests that the role of the dye in the recombination of electrons with the oxidized species might be important. It is reported that dyes can influence recombination in two ways: (1) they can block electrons in the metal oxide from reacting with acceptor species in the electrolyte,or (2) they can facilitate recombination through an association between the dye and triiodide.[55] The influence of dye structure on charge recombination has been highlighted recently.[54,56]

3.4. Open Circuit Voltage Decay and Lifetime Measurements. Open circuit voltage decay experiments were carried out to probe the recombination kinetics. Figure 4 shows the photovoltage transients for the three configurations in a semilogarithmic plot. According to Walker et al.[39] the photovoltage time decay should show a $\ln(t)$ dependence at longer times if recombination involves conduction band electrons that are detrapped from an exponential distribution of trapping states and a *quasi-static* state is maintained between free and trapped electrons. The logarithmic behavior in Figure 4 is also an indication that the back reaction via the substrate is negligible.[42] This is consistent with the fact that the voltage−illumination plots (Figure 1) are linear in the semilogarithmic plot.[23] According to Walker et al.[39] the slope in the $\ln(t)$ plot can be related to the trap distribution parameter α

$$\frac{dV_{oc}(t)}{d\ln t} \approx -\frac{k_B T/q}{1-\alpha} \quad (4)$$

The voltage versus $\ln(t - t_0)$ plots yield a similar slope for the three configurations studied. However, the decay is steeper than that predicted by the trap distribution parameter obtained from the capacitance measurements. This can be a further indication of nonlinear recombination, which can influence slope in the voltage−$\ln(t - t_0)$ plot as shown in the simulations reported in a previous work by the authors (see Supporting Information of ref 31).

The effective electron lifetime was obtained from three different techniques including OCVD and small perturbation measurements

$$\tau_n^{(IMVS)} = 1/\omega_{min} \quad (5)$$

$$\tau_n^{(OCVD)} = \frac{K_B T}{q}\left(\frac{dV_{oc}}{dt}\right)^{-1} \quad (6)$$

$$\tau_n^{(EIS)} = R_{ct} C_\mu \quad (7)$$

Electron lifetimes obtained from the three experimental techniques are presented in Figure 5. Once again the voltage has been corrected to account for band displacement for configuration C1

dx.doi.org/10.1021/jp206698t |J. Phys. Chem. C XXXX, XXX, 000–000

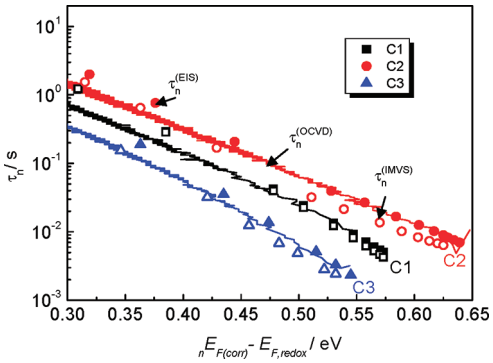

Figure 5. Electron lifetimes for the three cell configurations extracted from OCVD (lines), EIS (solid symbols), and IMVS (open symbols). Note that data for C1 have been corrected for band displacement according to the capacitance data of Figure 2.

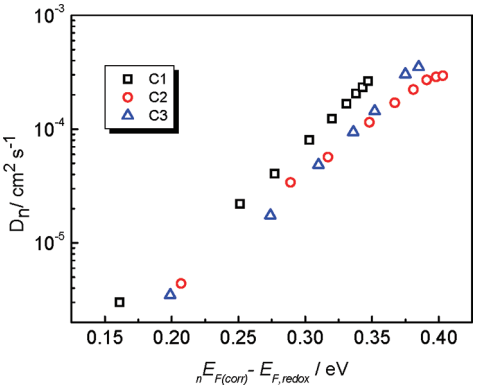

Figure 6. Diffusion coefficients for the three cell configurations obtained from the IMPS response. Note that data for C1 has been corrected for band displacement according to the capacitance data of Figure 2. The Fermi level position has been inferred from the measurement of the V_{sc} potential as indicated in the text and the Supporting Information.

as explained above. There is good agreement between the lifetimes extracted from the three techniques. Configuration C3 yields the shortest lifetime at the same position of the Fermi level. This explains the much smaller open circuit photovoltage found for this cell. Configuration C2 exhibits the longest lifetime, which explains its similar voltage to C1 despite the lack of TBP in the electrolyte.

According to eqs 2, 3, and 7, the lifetime versus the voltage should give an exponential with a characteristic exponent (with respect to k_BT/q) equal to $\alpha-\beta$. This is found to be approximately well fulfilled from lifetime measurements by EIS, IMVS, and OCVD. A comparison between the predicted values and the experimental results for each technique is summarized in Table S1 (Supporting Information).

3.5. Electron Transport. Electron transport properties in the nanostructured metal oxide were studied using intensity-modulated photocurrent spectroscopy (IMPS).[57,58] The spectra show the typical shape of an IMPS response for C1 and C2 over the complete range of intensities studied. However, for C3 an additional relaxation feature in the upper quadrant of the IMPS response appears at high light intensities (see Figure S4, Supporting Information). This behavior has been already reported for dye-sensitized solar cells where the iodine/iodide redox couple was substituted by a Co(dbbip)$_2$ redox shuttle and was attributed to diffusion limitation in the electrolyte.[59]

Assuming no recombination at short circuit, the time constant obtained from the imaginary minimum of the IMPS response can be related to the electron diffusion coefficient, D_n by[60,61]

$$\tau_{tr}^{(IMPS)} = \frac{d^2}{\gamma D_n} \tag{8}$$

where γ is a dimensionless factor that depends on the direction of illumination and ratio between the absorption length and the thickness of the film: αd[40,60] (see Figure S5, Supporting Information). In this work, we have used γ = 2.61, which corresponds to an absorption/thickness ratio of $\alpha d \sim 1$ (see Figure S5, Supporting Information). This value has been estimated from optical measurements of D149-sensitized ZnO electrodes previously reported by the authors.[31]

Short circuit voltage measurements[34] were used to estimate the Fermi level of electrons in the dye-sensitized semiconductor film when the cell is illuminated under short circuit conditions, as in an IMPS measurement. In Figure S6 in the Supporting Information the "short circuit" voltage V_{sc} measured at different light intensities is plotted together with the open circuit voltage for C1. This plot allows us to make an estimation of the quasi-Fermi level displacement at short circuit with respect to open circuit conditions. This shift is around 230 mV for configurations C1 and C2. A similar shift can be found in previous reports for ZnO[38] and TiO_2.[34] The shift for C3 is found to be smaller: 150 mV, which is consistent with the shorter electron lifetime for this type of cell.

In Figure 6, the diffusion coefficients for the three configurations are shown as a function of the position of the Fermi level. In this analysis, we have taken into account the conduction band shift for C1 mentioned above and the Fermi level displacement between open and short circuit conditions mentioned above. According to the multiple trapping model, the diffusion coefficient D_n should be related to the trap distribution parameter α through the expression[62−64]

$$D_n = D_0 \exp\left(\frac{(1-\alpha)({}_nE_F - E_{F,redox})}{k_BT}\right) \tag{9}$$

where D_0 is the diffusion coefficient in the dark. Therefore diffusion coefficients should increase with applied bias with a slope proportional to $(1-\alpha)q/k_BT$. However, D_n for the three cells exhibits a smaller slope that the one predicted from the distribution parameter obtained from the capacitance data, with α values ranging between 0.3 and 0.4. This anomalous behavior is discussed below in connection with the transport resistance inside the semiconductor film.

As already mentioned, it is difficult to extract reliable transport resistance values for ZnO solar cells in which the transmission line feature in the impedance spectra accounting for transport is not observed. In this work we have overcome this problem by combining IMPS and EIS data. As the time constant measured by IMPS can be used to obtain the diffusion coefficient, we can relate this to the product of the transport resistance of electron in the semiconductor film and the film capacitance.[64] Hence, according to eq 8, we can write

$$\tau_{tr}^{(IMPS)}\gamma = R_tC_\mu \tag{10}$$

Therefore, a way to obtain the transport resistance is to combine the time constant obtained from the IMPS measurements and the

dx.doi.org/10.1021/jp206698t |J. Phys. Chem. C XXXX, XXX, 000–000

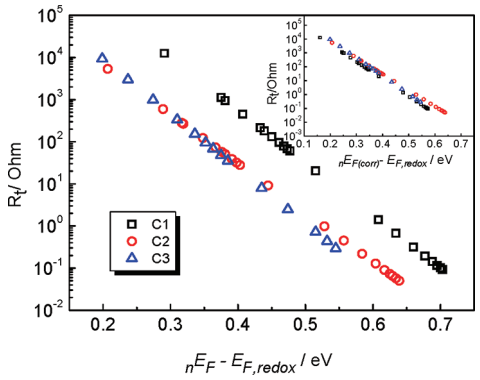

Figure 7. Transport resistance as obtained from the combination of EIS and IMPS measurements. Note that, in the inset, data for C1 have been corrected for band displacement according to the capacitance data of Figure 2.

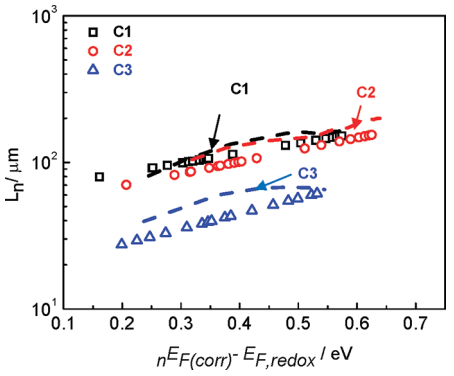

Figure 8. Small-perturbation electron diffusion lengths for the solar cells studied in this work from EIS ($(R_{ct}/R_t)^{1/2}$, dashed lines) and IMVS + IMPS ($(\tau_n D_n)^{1/2}$, symbols).

capacitance data obtained from the impedance response. However, it must be born in mind that to relate the characteristic time of the IMPS response to the transport resistance of the EIS transmission model is only an approximation, as the impedance theory is derived for homogeneous illumination (constant value of the distributed transport resistance).[64]

As IMPS is a short circuit measurement and EIS measurements was carried out at open circuit, the short circuit voltage measurements are necessary to relate the two parameters to the same trap occupancy (i.e., to the position of the Fermi level relative to the conduction band). In order to obtain a set of values for R_t in the range of interest, we fitted the IMPS time constant as a function of voltage to an exponential and extrapolated to obtain values in the same range of the capacitance data. The resulting transport resistances can be found in Figure 7. In the inset, the displacement for the conduction band shift has been corrected for. After this correction, all samples show a similar transport resistance, indicating that the conduction band offset obtained from the capacitance data for C1 is consistent with the shift observed in the transport resistance data. In Figure S7 in the Supporting Information, a comparison between the transport resistances obtained from this method and those obtained from the impedance fitting is shown for configuration C2. Reasonable agreement is found between the two methods at low voltages, but EIS values tend to flatten off at high Fermi levels. This is precisely the region where EIS fitting becomes less accurate.

In contrast to previous results for TiO_2 cells,[24,48,50] the behavior of the transport resistance (Figure 7) is not ideal with respect to Fermi level. Fabregat-Santiago et al.[48] found an ideal behavior of the transport resistance measured in the dark, but it departed from ideality when impedance measurements were carried out under illumination. The inverse slopes of the corresponding semilogarithmic plots are indicated in Table 2. The values range between 33 and 37 mV, i.e., considerably higher than the ideal value of 26 mV.

Several explanations can be proposed to account for the anomalous behavior of the transport properties. First of all, we must bear in mind that nonideality can arise from interactions between electrons[40,54] and these are more likely to be important in ZnO than in TiO_2 due to its lower dielectric constant. Nonideality in the transport was also found by Quintana et al.[38] and attributed to significant band bending present in the ZnO. However, as mentioned above, from the capacitance data we obtain a much lower charge density which would rule out any significant band bending.

3.6. Small Amplitude Electron Diffusion Length. For conditions of small perturbations with respect to a uniform background density, the electron diffusion length can be obtained from the effective values of the electron lifetime and the electron diffusion coefficient measured at coincident positions of the Fermi level[25,26,65]

$$L_n = \sqrt{\tau_n D_n} \tag{11}$$

As the diffusion coefficient is obtained from IMPS (short circuit) and the lifetime is obtained from IMVS (open circuit measurement), we have again to take into account the displacement of the Fermi level at short circuit with respect to open circuit so diffusion coefficients and lifetimes can be compared at the same values of the trap occupancy. Furthermore we have to correct for the band shift for configuration C1. A fit line to data was used to extrapolate and obtain a continuous function describing the relationship of D_n and τ_n with the electron quasi Fermi level along all the energy range of interest. The small amplitude diffusion lengths obtained from eq 11 are plotted in Figure 8 for the three types of cells.

The electron diffusion length can also be estimated from the EIS and IMPS data according to the expression[48,51]

$$\frac{L_n}{d} = \left(\frac{R_{ct}}{R_t}\right)^{1/2} \tag{12}$$

where R_{ct} is the charge transfer resistance and R_t is the electron transport resistance obtained by combining capacitance data and transport times from IMPS, as explained above. Results are also included in Figure 8. Good agreement is found between the two methods used to estimate the diffusion length.

The diffusion length is found to increase with voltage as it is expected for a nonlinear recombination mechanism.[25,26,65] The diffusion lengths are found to be much longer than the film thickness, indicating 100% collection efficiency. For ionic−liquid configuration (C3), the stronger recombination pointed out in the previous sections reduces the diffusion length significantly, but it is still considerably larger than the film thickness. The high values for the collection efficiency strongly suggest that low injection efficiency is the main cause of the limited performance of these solar cells.

3.7. Simulation of the *I*−*V* Curve and Implications in Cell Efficiency. The determination of transport and recombination

dx.doi.org/10.1021/jp206698t |J. Phys. Chem. C XXXX, XXX, 000–000

parameters makes it possible to attempt the simulation of the $I-V$ curves for the three configurations studied. To do so, we have solved numerically the continuity equation for electrons in the semiconductor film[66−68]

$$\frac{\partial n(x,t)}{\partial t} = G(x) + \frac{\partial}{\partial x}\left(D(n)\frac{\partial n(x,t)}{\partial x}\right) - k_R(n)n(x,t) \quad (13)$$

where $n(x,t)$ is the total density of electrons in the film as a function of distance to the front contact (x) and time (t), and $G(x)$ is an electron generation profile that involves the solar irradiance, the dye absorption spectrum, the quantum yield of electron injection, and the dye loading in the film (see Supporting Information). The continuity equation is solved for a density dependent diffusion coefficient $D(n)$ and a pseudo-first-order kinetic recombination constant $k_R(n)$. The density dependence of these magnitudes is related to their Fermi level dependence according to the experimental measurements in Figures 5 and 6 for the electron lifetime and the diffusion coefficient, respectively. Hence, the diffusion coefficient is modeled according to eq 9, whereas $k_R(n)$ (related to the inverse of the electron lifetime), is modeled via

$$k_R(n(x)) = k_R^0 \exp\left(\frac{(\beta-\alpha)({}_nE_F(x) - E_{F,redox})}{k_BT}\right) \quad (14)$$

where k_R^0 is adjusted to reproduce the experimental photovoltage at open circuit (note that n and E_F are functions of the spatial position x). Equation 14 can be obtained from the combination of eqs 2, 3, and 7, with the total density related to the photovoltage (${}_nE_F - E_{F,redox}$) via

$$n(x) = n_0 \exp\left(\frac{\alpha({}_nE_F - E_{F,redox})}{k_BT}\right) \quad (15)$$

where n_0 is the electron density in the dark. Note that eq 14 implies that the recombination rate is nonlinear in electron concentration, as it was recently discussed in refs 25 and 26 and it is inferred from our experimental results.

The continuity equation is solved in the space at time domain, and the photocurrent is obtained from the gradient of the total density profile at $x = 0$. The $I-V$ curve is simulated by solving the equation at various applied voltages at $x = 0$, from $V = 0$ (short circuit) to open circuit conditions, these defined the situation for which the photocurrent becomes zero (as stated above the parameter k_R^0 is adjusted to give zero current at the experimental open circuit voltage). The photocurrent is obtained once the steady-state condition is reached. The experimental short circuit photocurrent is matched by adjusting the dye loading in the film (assuming 100% injection quantum yield). The voltage drop due to series resistance is introduced by modifying the applied voltages by $V' \rightarrow V + JR_sA$, where A is the active area of the cell. The following common parameters were used to simulate the three configurations: $\alpha = 0.12$ (estimated from capacitance data), $\beta = 0.7$ (estimated from ideality factors, Table 2), $D_0 = 10^{-7}$ cm^2 s^{-1} (estimated from Figure 6) and $n_0 = 10^{15}$ cm^{-3}. Details of the calculation can be found in refs 66−68 and in the Supporting Information.

Results for the simulations are shown in Figure 9. When solving the equation with no series resistance, the resulting $I-V$ curve reproduces a nonideal diode with an ideality factor approximately equal to $1/\beta$ as can be seen in Figure 9 (dashed line) for C2. The values obtained for the adjustable parameter k_R^0 where 1.4×10^{-3}, 4×10^{-3}, and 3×10^{-2} s^{-1} for configurations C1, C2, and C3, respectively. These values allow us to obtain the pseudo-first-order recombination constant as a function of Fermi level using eq 14 and the $\beta-\alpha$ data of Table 2. The inverse of $k_R(n)$ is a pseudo-first-order electron lifetime. By making $E_F - E_{redox} = V_{oc}$ we obtain the following lifetimes: 1.9×10^{-3}, 5.1×10^{-3}, and 3.7×10^{-4} s, for configurations C1, C2, and C3, respectively. These predicted lifetimes are in good agreement with the experimental ones (Figure 5) for configurations C1 and C2, but not for C3 where the theoretical value is 1 order of magnitude smaller. In the case of C3, ion transport in the electrolyte is likely to have a significant contribution, which is ignored in this modeling. A more detailed model such as the one reported recently by Barnes et al.[54] is probably required to correctly simulate the $I-V$ curve in this case.

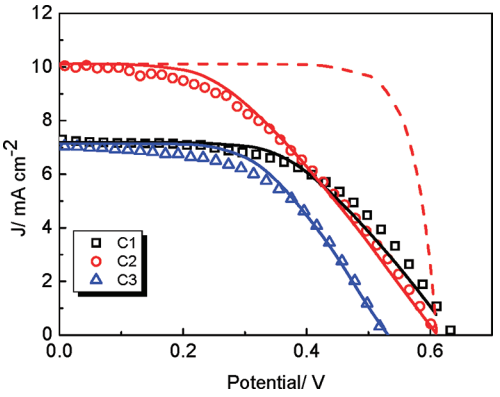

Figure 9. Experimental current−voltage curves for solar cells studied in this work (symbols) and simulations (lines). The simulation of C2 with no series resistance is also included (dashed line). See text and Supporting Information for details.

In Figure S8 of the Supporting Information the total density profiles and the Fermi level profiles for configuration C1 that arise from the numerical solution of the equation are shown. A Fermi level shift of 27 mV is predicted between short circuit and open circuit conditions. This value is quite close to the experimentally determined shift of 23 mV.

By fitting the photocurrent at the maximum power point, the series resistance acting in the cell can be extracted and the full $I-V$ curve reproduced. Values of $R_sA = 28.5$ Ω cm^2 were obtained for C1 and C2, and $R_sA = 20.5$ Ω cm^2 for C3. This resistance should correspond to the sum of the TCO resistance, the contribution of the counter-electrode, and the resistance of the electrolyte. These values are similar to those that can be extracted from the impedance spectra in Figure S2 (values of 25.1, 13.0, and 21.3 Ω cm^2 are obtained from EIS for C1, C2, and C3, respectively). The result of the modeling suggests that for the solar cells studied here series resistance has a more important influence on the low fill factor than the nonlinearity of the recombination kinetics.

Despite this result, additional effects may also have a contribution on the low fill factor of ZnO solar cells with respect to their TiO_2 counterparts. In this regard, Koops et al.[69] and more recently Cai et al.[28] have discussed the effect of applied bias on the electron injection yield. These authors report a decrease of the injection yield when the cell approaches open circuit conditions. Specifically, Cai et al. mentioned explicitly the effect of the back reaction (geminate recombination) between injected

dx.doi.org/10.1021/jp206698t |J. Phys. Chem. C XXXX, XXX, 000–000

electrons and oxidized dyes on the reduction of the injection efficiency. This effect might lead to an additional deterioration of the fill factor, which would be more important in the case of ZnO due to its lower dielectric constant. Jennings et al.[27] measured the IPCE/collection-efficiency ratio along the $I-V$ curve for a TiO_2-based cell and found a dramatic decrease at near open circuit conditions. This indicates that either injection or/and dye regeneration might become inefficient at high values of the Fermi level, lowering cell efficiencies and fill factors.

4. CONCLUSIONS

In this work we have studied the performance of ZnO-based dye solar cells with two different dyes and three different electrolytes. The following conclusions can be drawn from our results:

(1) Much larger IPCEs and photocurrents are obtained for the indoline dye, pointing to the importance of choosing a proper dye for ZnO and the limitations of the N719 for this semiconductor.

(2) Nonideality effects are observed both in recombination (EIS, lifetimes) and in transport properties (IMPS). The light-intensity dependence of the photovoltage for the three configurations exhibits nonideality factors very similar to those previously reported for TiO_2 cells. Nonideality in recombination can be attributed to nonlinear recombination kinetics. Nonideality in transport properties could arise from strong electron−electron interactions in the conduction band due to the lower dielectric constant of ZnO as compared with TiO_2.

(3) The voltage dependence of the capacitances as measured from EIS is weak, exponential, and very similar for the three configurations. According to the measured accumulated charge, band shift and band bending effects appear to be negligible for this kind of ZnO sample.

(4) The electron lifetimes extracted from IMVS, OCVD, and EIS show good agreement among the three techniques.

(5) Once corrected for band displacements, recombination resistances, lifetimes, and electron diffusion lengths indicate that solvent-free ionic−liquid electrolytes lead to significantly more rapid recombination kinetics compared with the other configurations. Even though no diffusion limitation is observed, the performance is lower than for the other two cells due to this feature.

(6) By combining EIS and IMPS data, it is possible to circumvent the problem of transport resistance determination when a clear transmission line feature is not observed in the impedance measurements.

(7) The electron diffusion length for the cells indicates good electron collection and an exponential increase with applied voltage that is indicative of nonlinear recombination. According to the diffusion lengths, a collection efficiency of 100% is expected.

(8) Low fill factors have a negative impact on the performance of the cells fabricated in this study. Numerical simulation of the $I-V$ curves indicates that this is mainly a consequence of the high series resistance (associated among other factors to large active area) than to nonideality effects. However, low injection efficiency or/and poor dye regeneration may also contribute to the low fill factor.

In summary, the behavior of ZnO dye solar cells can be described according to the same theories as in TiO_2 dye solar cells but with different characteristic parameters: smaller trap distribution parameter α, similar recombination reaction order, and stronger nonideal effects in the transport properties. However these differences do not lead to poor electron collection. If we consider that light harvesting in D149 cells is also very efficient, we conclude that the main limitations for ZnO for dye solar cells are related to the lack of an appropriate dye or to poor injection properties. In this regard recent reports[27−29,69] that emphasize the importance of electron−dye recombination and dye regeneration in the overall efficiency of the injection process suggest that the lower dielectric constant of ZnO might facilitate back reaction between injected electrons and oxidized dye molecules before these become regenerated by the redox pair.[70] In other words, charge separation might be more difficult to achieve in ZnO than in TiO_2, hence limiting performance dramatically. In this regard a comparative study between ZnO and TiO_2 devices with small series resistance is required.

■ ASSOCIATED CONTENT

Supporting Information. Figures showing incident photon to current efficiencies and IMPS data and numerical solution of the continuity equation. This material is available free of charge via the Internet at http://pubs.acs.org.

■ AUTHOR INFORMATION

Corresponding Author
*E-mail: anta@upo.es.

■ ACKNOWLEDGMENT

We thank the Ministerio de Ciencia e Innovación of Spain for funding under Project HOPE CSD2007-00007 (Consolider-Ingenio 2010) and CTQ2009-10477, and Junta de Andalucía under Projects P06-FQM-01869, P07-FQM-02595, and P07-FQM-02600.

■ REFERENCES

(1) Tributsch, H.; Gerischer, H. Elektrochemische Untersuchungen über den Mechanismus der Sensibilisierung und übersensibilisierung an ZnO-Einkristallen. *Ber. Bunsen-Ges. Phys. Chem.* **1969**, *73*, 251–260.

(2) O'Regan, B.; Grätzel, M. A low-cost, high-efficiency solar cell based on dye-sensitized colloidal TiO_2 films. *Nature* **1991**, *353*, 737–740.

(3) Tsubomura, H.; Matsumura, M.; Nomunara, Y.; Amamiya, T. Dye sensitised zinc oxide: aqueous electrolyte: platinum photocell. *Nature* **1976**, *261*, 402–403.

(4) Bauer, C.; Boschloo, G.; Mukhtar, E.; Hagfeldt, A. Electron Injection and Recombination in $Ru(dcbpy)_2(NCS)_2$ Sensitized Nanostructured ZnO. *J. Phys. Chem. B* **2001**, *105*, 5585–5588.

(5) Katoh, R.; Furube, A.; Yoshihara, T.; Hata, K.; Fujihashi, G.; Takano, S.; Murata, S.; Arakawa, H.; Tachiya, M. Efficiencies of Electron Injection from Excited N3 Dye into Nanocrystalline Semiconductor (ZrO_2, TiO_2, ZnO, Nb_2O_5, SnO_2, In_2O_3) Films. *J. Phys. Chem. B* **2004**, *108*, 4818–4822.

(6) Look, D. C.; Reynolds, D. C.; Sizelove, J. R.; Jones, R. L.; Litton, C. W.; Cantwell, G.; Harsch, W. C. Electrical properties of bulk ZnO. *Solid State Commun.* **1998**, *105*, 399–401.

(7) Seager, C. H.; Myers, S. M. Quantitative comparisons of dissolved hydrogen density and the electrical and optical properties of ZnO. *J. Appl. Phys.* **2003**, *94*, 2888–2894.

(8) Forro, L.; Chauvet, O.; Emin, D.; Zuppiroli, L.; Berger, H.; Levy, F. High mobility n-type charge carriers in large single crystals of anatase (TiO_2). *J. Appl. Phys.* **1994**, *75*, 633–635.

(9) Saito, M.; Fujihara, S. Large photocurrent generation in dye-sensitized ZnO solar cells. *Energy Environ. Sci.* **2008**, *1*, 280–283.
(10) Chiba, Y.; Islam, A.; Watanabe, Y.; Komiya, R.; Koide, N.; Han, L. Y. Dye-sensitized solar cells with conversion efficiency of 11.1%. *Jpn. J. Appl. Phys., Part 2* **2006**, *45*, L638–L640.
(11) Xu, F.; Sun, L. Solution-derived ZnO nanostructures for photoanodes of dye-sensitized solar cells. *Energy Environ. Sci.* **2011**, *4*, 818–841.
(12) Lai, Y.-H.; et al. Fabrication of a ZnO film with a mosaic structure for a high efficient dye-sensitized solar cell. *J. Mater. Chem.* **2010**, *20*, 9379–9385.
(13) Keis, K.; Bauer, C.; Boschloo, G.; Westermark, K.; Siegbahn, H. Nanostructured ZnO electrodes for dye-sensitized solar cell applications. *J. Photochem. Photobiol., A* **2002**, *148*, 57–64.
(14) Hochbaum, A. I.; Yang, P. Semiconductor Nanowires for Energy Conversion. *Chem. Rev.* **2010**, *110*, 527–546.
(15) González-Valls, I.; Lira-Cantú, M. Vertically-aligned nanostructures of ZnO for excitonic solar cells: a review. *Energy Environ. Sci.* **2009**, *2*, 19–34.
(16) Xu, F.; Dai, M.; Lu, Y.; Sun, L. Hierarchical ZnO Nanowire—Nanosheet Architectures for High Power Conversion Efficiency in Dye-Sensitized Solar Cells. *J. Phys. Chem. C* **2010**, *114*, 2776–2782.
(17) Hara, K.; Horiguchi, T.; Kinoshita, T.; Sugihara, H. Highly efficient photon-to-electron conversion with mercurochrome-sensitized nanoporous oxide semiconductor solar cells. *Sol. Energy Mater. Sol. Cells* **2000**, *64*, 115–134.
(18) Lee, W. J.; Okada, H.; Wakahara, A.; Yoshida, A. Structural and photoelectrochemical characteristics of nanocrystalline ZnO electrode with Eosin-Y. *Ceram. Int.* **2006**, *32*, 495–498.
(19) Guillén, E.; Casanueva, F.; Anta, J. A.; Vega-Poot, A.; Oskam, G.; Alcantara, R.; Fernández-Lorenzo, C.; Martín-Calleja, J. Photovoltaic performance of nanostructured zinc oxide sensitised with xanthene dyes. *J. Photochem. Photobiol., A* **2008**, *200*, 364–370.
(20) Oekermann, T.; Yoshida, T.; Minoura, H.; Wijayantha, K. G. U.; Peter, L. M. Electron Transport and Back Reaction in Electrochemically Self-Assembled Nanoporous ZnO/Dye Hybrid Films. *J. Phys. Chem. B* **2004**, *108*, 8364–8370.
(21) Oekermann, T.; Yoshida, T.; Boeckler, C.; Caro, J.; Minoura, H. Capacitance and Field-Driven Electron Transport in Electrochemically Self-Assembled Nanoporous ZnO/Dye Hybrid Films. *J. Phys. Chem. B* **2005**, *109*, 12560–12566.
(22) Galoppini, E.; Rochford, J.; Chen, H.; Saraf, H.; Lu, Y.; Hagfeldt, A.; Boschloo, G. Fast Electron Transport in Metal Organic Vapor Deposition Grown Dye-sensitized ZnO Nanorod Solar Cells. *J. Phys. Chem. B* **2006**, *110*, 16159–16161.
(23) Peter, L. M. Characterization and Modeling of Dye-Sensitized Solar Cells. *J. Phys. Chem. C* **2007**, *111*, 6601–6612.
(24) Wang, Q.; Ito, S.; Grätzel, M.; Fabregat-Santiago, F.; Mora-Seró, I.; Bisquert, J.; Bessho, T.; Hachiro, I. Characteristics of high efficiency dye-sensitized solar cells. *J. Phys. Chem. B* **2006**, *110*, 25210–25221.
(25) Bisquert, J.; Mora-Seró, I. Simulation of Steady-State Characteristics of Dye-Sensitized Solar Cells and the Interpretation of the Diffusion Length. *J. Phys. Chem. Lett.* **2010**, *1*, 450–456.
(26) Villanueva-Cab, J.; Wang, H.; Oskam, G.; Peter, L. M. Electron Diffusion and Back Reaction in Dye-Sensitized Solar Cells: The Effect of Nonlinear Recombination Kinetics. *J. Phys. Chem. Lett.* **2010**, *1*, 748–751.
(27) Jennings, J. R.; Liu, Y.; Wang, Q. Efficiency Limitations in Dye-Sensitized Solar Cells caused by Inefficient Sensitizer Regeneration. *J. Phys. Chem. C* **2011**, *115*, 15109–15120.
(28) Cai, J.; Satoh, N.; Han, L. Injection Efficiency in Dye-Sensitized Solar Cells within a Two-Band Model. *J. Phys. Chem. C* **2011**, *115*, 6033–6039.
(29) Barnes, P. R. F.; Andersson, A. Y.; Juozapavicius, M.; Liu, L.; Li, X.; Palomares, E.; Forneli, A.; ÓRegan, B. Factors controlling charge recombination under dark and light conditions in dye sensitised solar cells. *Phys. Chem. Chem. Phys.* **2011**, *13*, 3547–3558.
(30) Guillén, E.; et al. ZnO-based dye solar cell with pure ionic-liquid electrolyte and organic sensitizer: the relevance of the dye-oxide interaction in an ionic-liquid medium. *Phys. Chem. Chem. Phys.* **2011**, *13*, 207–213.
(31) Guillén, E.; Azaceta, E.; Peter, L. M.; Arnost, Z.; Tena-Zaera, R.; Anta, J. A. ZnO solar cells with an indoline sensitizer: a comparison between nanoparticulate films and electrodeposited nanowire arrays. *Energy Environ. Sci.* **2011**, *4*, 3400–3407.
(32) Elías, J.; Tena-Zaera, R.; Lévy-Clément, C. Electrodeposition of ZnO nanowires with controlled dimensions for photovoltaic applications: Role of buffer layer. *Thin Solid Films* **2007**, *515*, 8553–8557.
(33) Ito, S.; Matsui, H.; Okada, K.; Kusano, S.; Kitamura, T.; Wada, Y.; Yanagida, S. Calibration of solar simulator for evaluation of dye-sensitized solar cells. *Sol. Energy Mater. Sol. Cells* **2004**, *82*, 421–429.
(34) Boschloo, G.; Hagfeldt, A. Activation Energy of Electron Transport in Dye-Sensitized TiO_2 Solar Cells. *J. Phys. Chem. B* **2005**, *109*, 12093–12098.
(35) Horiuchi, T.; Miura, H.; Sumioka, K.; Uchida, S. High Efficiency of Dye-Sensitized Solar Cells Based on Metal-Free Indoline Dyes. *J. Am. Chem. Soc.* **2004**, *126*, 12218–12219.
(36) Guillén, E.; Fernández-Lorenzo, C.; Alcántara, R.; Martín-Calleja, J.; Anta, J. A. Solvent-free ZnO dye-sensitised solar cells. *Sol. Energy Mater. Sol. Cells* **2009**, *93*, 1846–1852.
(37) Keis, K.; Magnusson, E.; Lindstrom, H.; Lindquist, S. E.; Hagfeldt, A. A 5% efficient photo electrochemical solar cell based on nanostructured ZnO electrodes. *Sol. Energy Mater. Sol. Cells* **2002**, *73*, 51–58.
(38) Quintana, M.; Edvinsson, T.; Hagfeldt, A.; Boschloo, G. Comparison of dye-sensitized ZnO and TiO_2 solar cells: studies of charge transport and carrier lifetime. *J. Phys. Chem. C* **2007**, *111*, 1035–1041.
(39) Walker, A. B.; Peter, L. M.; Lobato, K.; Cameron, P. J. Analysis of Photovoltage Decay Transients in Dye-Sensitized Solar Cells†. *J. Phys. Chem. B* **2006**, *110*, 25504–25507.
(40) Jennings, J. R.; Ghicov, A.; Peter, L. M.; Schmuki, P.; Walker, A. B. Dye-sensitized solar cells based on oriented TiO_2 nanotube arrays: Transport, trapping, and transfer of electrons. *J. Am. Chem. Soc.* **2008**, *130*, 13364–13372.
(41) O'Regan, B. C.; Durrant, J. R. Kinetic and Energetic Paradigms for Dye-Sensitized Solar Cells: Moving from the Ideal to the Real. *Acc. Chem. Res.* **2009**, *42*, 1799–1808.
(42) Cameron, P. J.; Peter, L. M.; Hore, S. How Important is the Back Reaction of Electrons via the Substrate in Dye-Sensitized Nanocrystalline Solar Cells?. *J. Phys. Chem. B* **2005**, *109*, 930–936.
(43) Bisquert, J. Chemical capacitance of nanostructured semiconductors: its origin and significance for nanocomposite solar cells. *Phys. Chem. Chem. Phys.* **2003**, *5*, 5360–5364.
(44) Wang, H.; Peter, L.M. A Comparison of Different Methods To Determine the Electron Diffusion Length in Dye-Sensitized Solar Cells. *J. Phys. Chem. C* **2009**, *113*, 18125–18133.
(45) Hagfeldt, A.; Grätzel, M. Light-Induced Redox Reactions in Nanocrystalline Systems. *Chem. Rev.* **1995**, *95*, 49–68.
(46) *Dye-Sensitized Solar Cells*; Kalyanasundaram, K., Ed.; EPFL Press: Lausanne, 2010.
(47) Watson, D. F.; Meyer, G. J. Cation effects in nanocrystalline solar cells. *Coord. Chem. Rev.* **2004**, *248*, 1391–1406.
(48) Fabregat-Santiago, F.; Bisquert, J.; Garcia-Belmonte, G.; Boschloo, G.; Hagfeldt, A. Influence of electrolyte in transport and recombination in dye-sensitized solar cells studied by impedance spectroscopy. *Sol. Energy Mater. Sol. Cells* **2005**, *87*, 117–131.
(49) González-Pedro, V.; Xu, X.; Mora-Seró, I.; Bisquert, J. Modeling High-Efficiency Quantum Dot Sensitized Solar Cells. *ACS Nano* **2010**, *4*, 5783–5790.
(50) Wang, M.; Chen, P.; Humphry-Baker, R.; Zakeeruddin, S. M.; Grätzel, M. The Influence of Charge Transport and Recombination on the Performance of Dye-Sensitized Solar Cells. *ChemPhysChem* **2009**, *10*, 290–299.
(51) Bisquert, J. Theory of the Impedance of Electron Diffusion and Recombination in a Thin Layer. *J. Phys. Chem. B* **2002**, *106*, 325–333.

(52) Boschloo, G.; Edvinsson, T.; Hagfeldt, A. Dye-sensitized nanostructured ZnO electrodes for solar cell applications. *Nanostruct. Mater. Sol. Energy Convers.* **2006**, 227–254.

(53) Bisquert, J.; Vikhrenko, V. S. Interpretation of the Time Constants Measured by Kinetic Techniques in Nanostructured Semiconductor Electrodes and Dye-Sensitized Solar Cells. *J. Phys. Chem. B* **2004**, *108*, 2313–2322.

(54) Barnes, P. R. F.; Anderson, A. Y.; Durrant, J. R.; O'Regan, B. C. Simulation and measurement of complete dye sensitised solar cells: including the influence of trapping, electrolyte, oxidised dyes and light intensity on steady state and transient device behaviour. *Phys. Chem. Chem. Phys.* **2011**, *13*, 5798–5816.

(55) Hagfeldt, A.; Boschloo, G.; Sun, L.; Kloo, L.; Pettersson, H. Dye-sensitized solar cells. *Chem. Rev.* **2010**, *110*, 6595–6663.

(56) Jennings, J. R.; Liu, Y.; Wang, Q.; Zakeeruddin, S. M.; Gratzel, M. The influence of dye structure on charge recombination in dye-sensitized solar cells. *Phys. Chem. Chem. Phys.* **2011**, *13*, 6637–6648.

(57) Cao, F.; Oskam, G.; Meyer, G. J.; Searson, P. C. Electron Transport in Porous Nanocrystalline TiO_2 Photoelectrochemical Cells. *J. Phys. Chem.* **1996**, *100*, 17021–17027.

(58) Fisher, A. C.; Peter, L. M.; Ponomarev, E. A.; Walker, A. B.; Wijayantha, K. G. U. Intensity Dependence of the Back Reaction and Transport of Electrons in Dye-Sensitized Nanocrystalline TiO_2 Solar Cells. *J. Phys. Chem. B* **2000**, *104*, 949–958.

(59) Wang, H.; Nicholson, P. G.; Peter, L.; Zakeeruddin, S. M.; Grätzel, M. Transport and Interfacial Transfer of Electrons in Dye-Sensitized Solar Cells Utilizing a $Co(dbbip)_2$ Redox Shuttle. *J. Phys. Chem. C* **2010**, *114*, 14300–14306.

(60) Dloczik, L.; Ileperuma, O.; Lauermann, I.; Peter, L. M.; Ponomarev, E. A.; Redmond, G.; Shaw, N. J.; Uhlendorf, I. Dynamic Response of Dye-Sensitized Nanocrystalline Solar Cells: Characterization by Intensity-Modulated Photocurrent Spectroscopy. *J. Phys. Chem. B* **1997**, *101*, 10281–10289.

(61) Lagemaat, J. van de; Frank, A. J. Nonthermalized electron transport in dye-sensitized nanocrystalline TiO_2 films: Transient photocurrent and random-walk modeling studies. *J. Phys. Chem. B* **2001**, *105*, 11194–11205.

(62) Anta, J. A.; Mora-Seró, I.; Dittrich, T.; Bisquert, J. Interpretation of diffusion coefficients in nanostructured materials from random walk numerical simulation. *Phys. Chem. Chem. Phys.* **2008**, *10*, 4478–4485.

(63) Ito, S.; Zakeeruddin, S. M.; Humphry-Baker, R.; Liska, P.; Charvet, R.; Comte, P.; Nazeeruddin, M. K.; Pechy, P.; Takata, M.; Miura, H.; Uchida, S.; Grätzel, M. High-efficiency organic-dye-sensitized solar cells controlled by nanocrystalline-TiO_2 electrode thickness. *Adv. Mater.* **2006**, *18*, 1202–1205.

(64) Bisquert, J. Theory of the Impedance of Electron Diffusion and Recombination in a Thin Layer. *J. Phys. Chem. B* **2002**, *106*, 325–333.

(65) Jennings, J. R.; Li, F.; Wang, Q. Reliable Determination of Electron Diffusion Length and Charge Separation Efficiency in Dye-Sensitized Solar Cells. *J. Phys. Chem. C* **2010**, *114*, 14665–14674.

(66) Villanueva, J.; Anta, J. A.; Guillén, E.; Oskam, G. Numerical Simulation of the Current−Voltage Curve in Dye-Sensitized Solar Cells. *J. Phys. Chem. C* **2009**, *113*, 19722–19731.

(67) Villanueva-Cab, J.; Oskam, G.; Anta, J. A. A simple numerical model for the charge transport and recombination properties of dye-sensitized solar cells: A comparison of transport-limited and transfer-limited recombination. *Sol. Energy Mater. Sol. Cells* **2010**, *94*, 45–50.

(68) Anta, J. A.; Casanueva, F.; Oskam, G. A numerical model for charge transport and recombination in dye-sensitized solar cells. *J. Phys. Chem. B* **2006**, *110*, 5372–5378.

(69) Koops, S. E.; O'Regan, B. C.; Barnes, P. R. F.; Durrant, J. R. Parameters Influencing the Efficiency of Electron Injection in Dye-Sensitized Solar Cells. *J. Am. Chem. Soc.* **2009**, *131*, 4808–4818.

(70) Anderson, A. Y.; Barnes, P. R. F.; Durrant, J. R.; O'Regan, B. C. Quantifying Regeneration in Dye-Sensitized Solar Cells. *J. Phys. Chem. C* **2011**, *115*, 2439–2447.